Acta Cryst. (1959). **12**, 313

Microcleavage, Bonding Character and Surface Structure in Materials with Tetrahedral Coordination

By G. A. Wolff and J. D. Broder

U.S. Army Signal Research & Development Laboratory, Fort Monmouth, N. J., U.S.A.

(*Received* 29 *May* 1958)

The investigation of microcleavage, defined as the separation of crystals parallel to certain crystallographic directions, proves useful for detecting atomic arrays held together by strong bonds (*PBC* vectors). Estimates of ionic and covalent bonding character can be made and surface properties can be investigated.

A structural collapse of the crystal surface layers in some materials with a low coordination (Si, Ge; HgSe, HgTe; $AuGa_2$, $AuIn_2$), is indicated for certain crystal planes. For Si and Ge, these results confirm earlier data on crystal habit and corroborate a similar hypothesis proposed by Schlier & Farnsworth (1956) from low-energy electron diffraction data.

1. Introduction

In compounds $A(n)B(8-n)$ having sphalerite and wurtzite structures, the effective electronic charge q/e of the constituents A and B varies between the values $\pm n$ and $\pm(n-4)$* (+ refers to A and − refers to B). The latter limits are indicative of ionic and covalent bonding as in $Ga^{3+}P^{3-}$ and $Ga^{-}P^{+}$ respectively. Since the electronic and semiconductor properties of these materials are a function of q/e, attempts have been made to determine the amount of ionic character in sphalerite or wurtzite structure crystals. The methods used include infrared measurements (Szigeti, 1949; Spitzer & Fan, 1955; Picus, Burstein & Henvis, 1956; Burstein & Egli, 1955) electron-density mapping (Jeffrey & Perry, 1955; Jeffrey, Perry & Mozzi, 1956) paramagnetic resonance (Van Wieringen, 1955) and a correlation of empirical data (Goodman, 1954, 1955).

There is another technique by which we can obtain information, in a simple manner, of the bonding character in sphalerite structure materials, and that is by the investigation of cleavage. Crystals of sphalerite structure, with an effective electronic charge $q/e \neq 0$ of the surface atoms, are expected to cleave in (011) as in sphalerite, and with 'neutral' bulk bonding ($q/e = 0$) they are expected to cleave along (111) as does diamond (Winkler, 1950). Thus, from the ratio of (011) to (111) cleavage, we should be able to learn about the bonding character of materials with sphalerite structure (Wolff, 1954; Pfister, 1955).

In the course of this study, an unexpected type of cleavage was found which could not be explained by the foregoing principles but only by atomic displacements within the surface layers of the materials being studied. Since this information aids in understanding the surface behavior of semi-conductors, the latter is also included in this work.

* The number n indicates the group of the constituent on the periodic chart, e.g. for B, Al, Ga, In, n is 3; for Be, Mg, Zn, Cd, Hg, n is 2, etc.

2. Macrocleavage and microcleavage

The principles that determine a plane of cleavage are as follows:

1. The number of 'bonds' (nearest neighbors) to be separated per unit area of the plane is a minimum, as compared to all other crystal planes.
2. The plane is electrically neutral with alternate arrays of positive and negative structure elements ('checker board arrangement') which permit the two separating surface layers to assume repelling positions when shifted with respect to each other. For materials with diamond and sphalerite structure, conditions 1 and 2 require (111) and/or (011) cleavage (Winkler, 1950).

Previously, by employing the 'razor-blade' technique, cleavage in (011) was found in all antimonides, arsenides and phosphides of In, Ga and Al; in addition (111) cleavage was detected in InSb, InAs, InP* and GaSb (Wolff, 1954). Thus, on the basis of this principle, it was possible to verify the presence of covalent bonding in the latter compounds.

By conventional goniometric methods only macroscopic cleavage is normally recorded, that is, cleavage planes of at least 0·1 mm. in diameter; while other types of 'fracture' are listed as conchoidal, subconchoidal 'hackle', and so on.† The microcleavage technique gives more detailed information, however. As far as we know, there is no reported attempt to record 'microcleavage' parallel to certain crystallographic directions. This includes 'macrocleavage' as well, which is found mostly at intersections of at least two such 'microcleavage' zones.

This is demonstrated in Fig. 1, where a cube of the

* Cleavage in InP was not mentioned in the abstract.

† The appearance of the fracture patterns gives evidence for dislocations and the fracturing force as it traverses the crystal (Zapffe & Worden, 1949; Mitrenin & Alexandria, 1957).

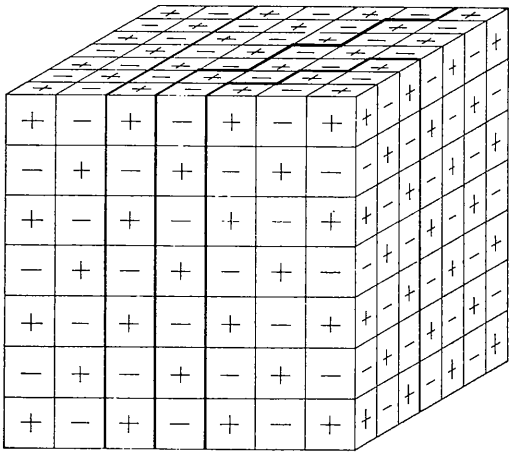

Fig. 1. Model of NaCl structure crystal. Heavy lines indicate (010), (120) and (110) cleavage planes if the corresponding parts on either side of the heavy lines are shifted vertically in opposite directions.

NaCl structure is shown. By a vertical shift of the crystal part on the right of the heavy lines with respect to the corresponding remainder of the crystal on the left, (010), (120) or (110) cleavage occurs, or, in general, microcleavage in (*hk*0) parallel to the [001] axis. This is to be expected, since repelling forces are activated during the shift with ions of like charge coming into opposing positions. Of these cleavages, only (010) and (110) have been observed in NaCl (Winkler, 1950), LiF, KBr and MgO as 'macrocleavage'. By means of the 'light figure' technique (Wolff, Wilbur, Jr., & Clark, 1957), however, all other 'microcleavage' planes (*hk*0) have also been found in these materials. The light figure of these materials is identical to the light figure of HgTe shown in Fig. 4(*b*). In PbS, PbTe and SnSe only (010) macrocleavage was observed.

The appearance of (111) 'macrocleavage' (flat portions of the surface) and (*hhl*) 'microcleavage' (cylindrically curved portions of the surface) in Si and diamond is shown in the electronmicrographs (Figs. 2 and 3). In these micrographs, the cleavage planes in the [1$\bar{1}$0] zone appear as true planes and not as an arrangement of submicroscopic steps of (111) planes. In rare instances, only the microcleavage would appear in macroscopic size*, although usually they would not be of any appreciable dimension. In the corresponding light figure photographs, microcleavage is represented by linear or curved zonal reflections of a series of microcleavage planes parallel to certain crystallographic zones, and macrocleavage is represented either by an intersection of at least two such zonal microcleavage reflections (e.g. (111) in Figs. 4 and 5) or by reflections that are distinct and more intense than their neighboring planes (e.g. (110) in Figs. 4(*a*), (*b*), (*c*)).

* For example see Dewald (1955, 1957) and Ramaseshan (1946).

3. Experimental technique used in the investigation of microcleavage

The microcleavage was investigated in three ways:

(1) The single crystal spheres were 'ground' with a wet slurry, consisting of SiC (240 or 150 mesh), on the end of a vertical brass pipe, the diameter of which was about $\frac{3}{4}$ that of the sphere. The pipe rotated at a moderate speed. For most of the materials investigated, water was the wetting agent in the slurry, although it was necessary to use oil when moisture-sensitive compounds such as AlSb, Mg_2Sn, NaCl, KBr were studied. A 120-mesh diamond grinding wheel was used to treat diamond and SiC crystal spheres. Also, a Si sphere was treated with 50-mesh Si particles on a plastic substrate.

While this technique could be described as a grinding or abrading technique, there is one essential difference which makes it applicable to the investigation of microcleavage of brittle materials. The use of *coarse* grinding particles of 240-mesh or larger makes it possible to cleave or chip minute pieces from the surface of the investigated crystals, leaving innumerable tiny 'cleavage pits' in the surface. The planes which make up these pits are the result of both macro- and microcleavage.

This can be demonstrated optically by reflection measurements from these cleavage planes. Of course, in addition to cleavage, there is some abrasive action resulting from the above method of preparation. Therefore, the following technique was used to minimize this undesirable effect.

(2) The crystal spheres under investigation were bounced off the interior wall of a SiC wheel modified after Bond (1951). The wheel carries sharp, free SiC grit of comparable size. It is by this method that the (11$\bar{2}$0) cleavage in CdS, CdSe and the microcleavage, near (011) in Si and Ge, is developed. These cleavages are just barely visible, using method 1.

(3) Both methods 1 and 2 are excellent for brittle materials, but they are not good for soft materials such as $AuIn_2$, $AuGa_2$, InBi, CsBr and Bi, which show slipping. For these fairly soft materials which are, however, still brittle enough to allow cleavage when broken by the sudden application of shock or force, a third method is applicable. In this method, single crystal plates are held in a vise, or supported at two points, then broken by the sudden application of a load, which is done quickly in order to avoid plastic deformation. The fracture surface shows essentially the same light figure pattern as that obtained by either method (1) or (2). In a few cases, there is a certain amount of bending or other plastic deformation of the crystal. This is readily discernible in the light figure pattern. The use of low temperatures extends the applicability range of this method to other materials which cannot be cleaved effectively at room temperature, as for instance, Bi.

Before being subjected to the light figure investiga-

Fig. 2. Electronmicrograph of the surface of a fractured Si single crystal (negative of shadowed replica). The area at the upper left shows a (111) cleavage, the dark steps at the lower right represent mostly (111), while the tilt of these steps on the light portions seems to be toward (100). In other words the apparently curved section would represent (*hhl*) with $h < l$.

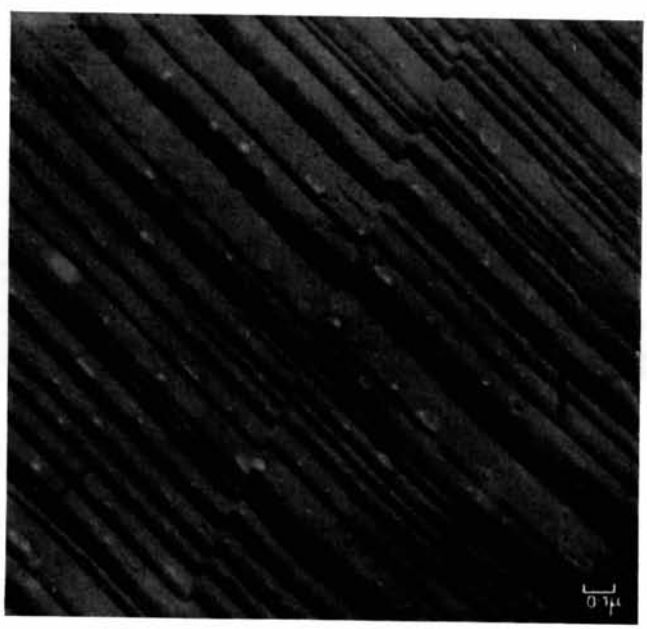

Fig. 3. Electronmicrograph of the surface of a diamond '(110) cleavage' (positive of shadowed replica). The lines going from the upper left to the lower right follow the $[1\bar{1}0]$ direction. The flat lightest and darkest portions of the steps following this direction correspond to (111) and $(11\bar{1})$ cleavage, while the curved portions of intermediate darkness represent parts of (*hhl*) planes with $h > l$. The offset along the line going from the upper right to the lower left, following the $[1\bar{1}4]$ direction, may represent a component of a slip (possibly in (113) or (115)). The slip is the only one found on an area $\frac{1}{2}$ by $\frac{3}{4}$ cm. It is not pertinent to the cleavage.

[*To face p.* 314

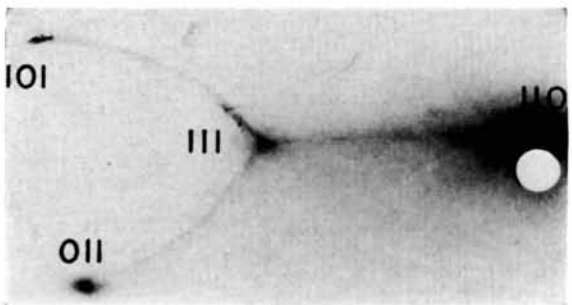

(a)

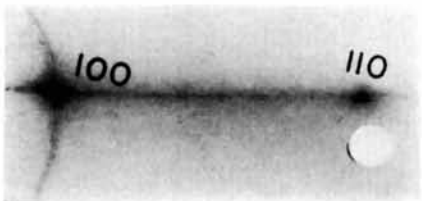

(b)

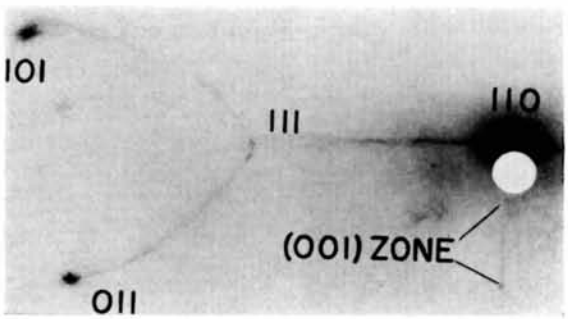

(c)

Fig. 4. Light figure cylinder reflections from rough-ground single crystal spheres of (*a*) InSb, (*b*) HgTe and (*c*) CdTe. The dark lines represent microcleavage planes and zones shown also in the schematic diagram in Figs. 6 and 7.

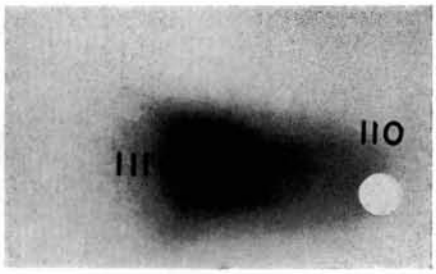

(a)

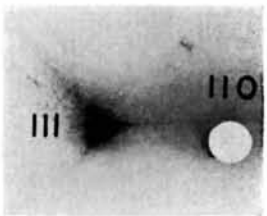

(b)

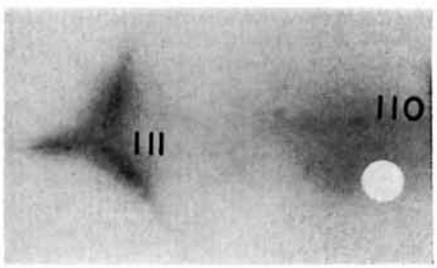

(c)

Fig. 5. Light figure reflections of single crystal spheres of (*a*) diamond, (*b*) Sb_4O_6 and (*c*) Si. The reflections of the diamond are fuzzy due to the fact that diamond could not be ground with a material harder than diamond, therefore, the resulting planes of the 'cleavage' pits are only of small size. The corresponding light figure reflection from the surface in Fig. 3, however, is very distinct.

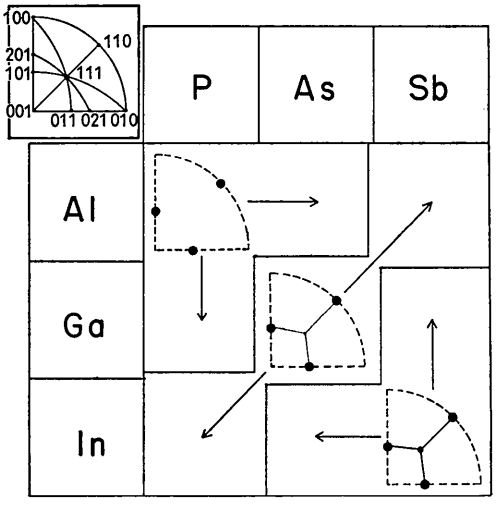

Fig. 6. The stereographic projections of the cleavage and microcleavage of the III–V compounds. The dotted lines represent the outline of the areas projected and indicate no cleavage data. Arrows point to the places where the stereographic diagram also holds. A corresponding model of the stereographic projection indicating planes and zones for Figs. 6, 7, 8 and 10 is shown in the legend in the upper left.

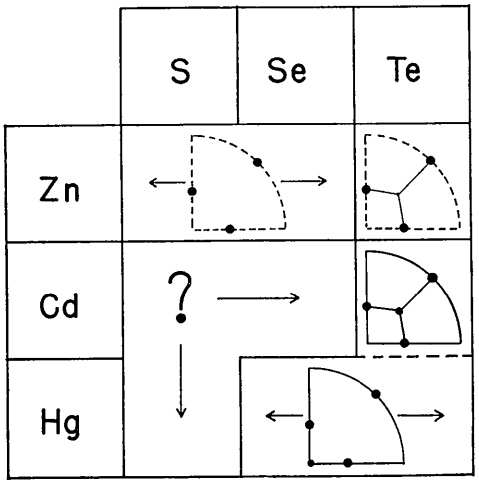

Fig. 7. The stereographic projections of the cleavage and microcleavage of the II–VI compounds with sphalerite structure. The question marks in the places for CdS, CdSe and HgS indicate cleavage properties unknown so far, since the crystals cannot be grown to appreciable size (CdS, CdSe) or good crystals for this purpose were not available (metacinnabarite specimens). Arrows in the upper and lower rows indicate identical patterns for ZnS and ZnSe; and for HgSe and HgTe, respectively. Notice the (001) cleavage and [100] microcleavage in HgSe, HgTe and CdTe.

tion, all transparent materials were covered with evaporated layers of metal to get better reflection. The spheres were rolled on a watch glass during evaporation, while crystals of other shapes were fastened to hemispheres and rocked back and forth. Au, Ag, and Al were chosen as evaporating metals so as to avoid solid state reaction between metal layer and crystal substrate.

4. Experimental cleavage patterns

(*a*) *Sphalerite-structure materials*

AlP, AlAs, AlSb, GaP, GaAs, GaSb, InP, InAs, InSb, ZnS, ZnSe, ZnTe, CdTe, HgSe, HgTe and CuI have been studied. AlP and AlAs crystals, which were small in size ($2\times2\times0{\cdot}5$ mm.), have been investigated by the 'razor-blade' technique only. All these compounds show distinct (011) cleavage. In the text which follows, this will be called Type 1 Cleavage. AlSb, GaAs, InP, ZnTe, and to a greater extent, GaSb, InAs, InSb (Fig. 4(*a*)) and CdTe (Fig. 4(*c*)), also show microcleavage in the planes $(hhl)(h \geq l)$. This will be called Type 2 Cleavage (Figs. 5(*a*), (*b*)). Only a few typical microcleavage reflection photographs have been selected and are shown. In HgSe and HgTe, on the other hand, microcleavage in all planes of zone [001] (called Type 3 Cleavage (Fig. 4(*b*)) has been found, in addition to the distinct cleavage in (011). All three types of cleavage cited have been discerned in CdTe (Fig. 4(*c*)). The corresponding stereographic projections (Figs. 6, 7) illustrate these experimental results.

For simplicity, the following cleavage has not been recorded in the stereographic projections: (111) in HgSe; (111) in InP, which is more pronounced than is indicated in Fig. 6; and microcleavage often found in planes parallel to the [111] zone together with very little or no cleavage in (111). These data contribute only to a refinement of the analysis and their omission will have no particular influence on the conclusions drawn. It should be noted that for both CdTe and ZnTe crystals of high purity, only (011) and [111] cleavage was observed. This will be explained later. The structurally related tetragonal chalcopyrite $CuFeS_2$ shows cleavage properties similar to those of InSb (Fig. 8), and distinct (011) cleavage and micro-

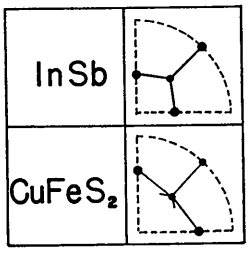

Fig. 8. The stereographic projections of the cleavage and microcleavage of $CuFeS_2$. The pattern of the InSb is given for comparison.

cleavage between (011) and (112) which correspond to (021) and (111) if indexed as a cubic crystal (referred to as 'cubic notation' below).

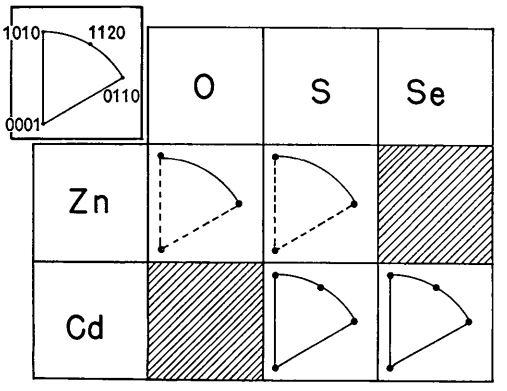

Fig. 9. The stereographic projections of the II–VI compounds with hexagonal wurtzite structure. The shaded areas indicate the inexistence of this structure. Notice the difference in the cleavage and microcleavage between the Zn and Cd compounds. The planes are shown in the legend in the upper left.

(b) Wurtzite-structure materials

ZnO, ZnS, CdS, CdSe and AgI were studied (Fig. 9) ZnO and ZnS show cleavage in (0001) and $(10\bar{1}0)$ and microcleavage in all prism planes ([0001] zone); the reflection patterns of CdS and CdSe show, in addition, distinct $(11\bar{2}0)$ cleavage and microcleavage between (0001) and $(10\bar{1}0)$, $([01\bar{1}0])$. Distinct (0001) cleavage and microcleavage parallel to $[01\bar{1}0]$ were also found in AgI crystals, but repeated attempts to find cleavage or microcleavage in a prismatic plane were unsuccessful. This may be due to the fact that the AgI crystals were too small (2–3 mm.). The same result as in AgI was obtained for hexagonal SiC. Some time and effort has been spent on the investigation of hexagonal (tridymite) ice, which has a structure related to wurtzite. Ice spheres 4–6 mm. in diameter were prepared from larger specimens and have been studied in a cold chamber at −20 °C. Since a metal evaporation technique could not be employed, and since in some cases the spheres may not have been single crystals, the results were inconclusive. A 90° angle between cleavage planes was found. Results obtained on large, single, naturally-grown crystal plates and long, solid, and tubular prisms, by conventional cleavage technique, prove (0001) and $(10\bar{1}0)$ to be cleavage planes.

(c) Fluorite-structure materials

CaF_2 and Mg_2Sn single crystal spheres display (111) cleavage and microcleavage between (111) and (110) which is identical to pattern 2 (Figs. 5(*a*), (*b*) and 10). Single crystals of $AuGa_2$ and $AuIn_2$ show this pattern together with the pattern of Type 3.

(d) Diamond-structure materials

In diamond there is good (111) cleavage and microcleavage between (111) and (110) parallel to the $[1\bar{1}0]$ zone, (Figs. 5(*a*), 10). The same result is observed in the molecular diamond structure materials As_4O_6 and Sb_4O_6 (arsenolite and senarmontite; Fig. 5(*b*)). Si and Ge display a different cleavage namely good (111) cleavage, a residual microcleavage in and near (110), and microcleavage between (111) and (001) in the $[1\bar{1}0]$ zone. Since the diamond sphere was treated with coarse diamond particles (of the same hardness), only very small exposures of the cleavage and microcleavage planes were obtained. Therefore, in the light reflections the percentage of diffraction is high and diffuse light figures result. The corresponding reflection from the '(110)' cleavage obtained by 'cutting' a diamond is very distinct, however.

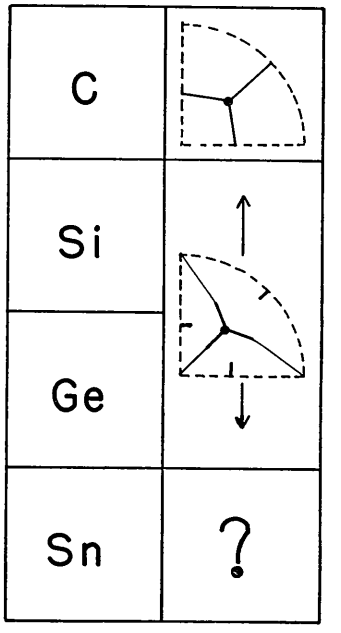

Fig. 10. The stereographic projections of the cleavage and microcleavage of diamond, silicon and Ge. Single crystals of grey tin of sufficient size were not available at the moment. Notice the difference between diamond, on the one hand, and of silicon and germanium, on the other.

(e) Materials with structural vacancies

Materials of this type, such as Ga_2Te_3, In_2Te_3, Cu_3AsS_3 (tennantite), Cu_3SbS_3 (tetrahedrite), $HgIn_2Te_4$ and $NiIn_2$, seldom show distinct cleavage. Of these materials, only Ga_2Te_3 and In_2Te_3 have a distinct (111) cleavage. Cu_3AsS_3 and Cu_3SbS_3 show only indistinct (011) cleavage. In all other such materials, neither cleavage nor microcleavage was found. In contrast, Cu_3AsS_4 (enargite) which has no vacancies shows distinct macro- and microcleavage.

5. Discussion

(a) Sphalerite-structure materials

(i) Ionic and covalent bonding in the bulk.

There is no doubt that the bonding in diamond structure materials (diamond, Si, Ge, α-Sn) is covalent in nature. However, the bonding in $A(n)B(8-n)$ materials having sphalerite and wurtzite structures is not purely ionic, i.e. it is not a bonding between cations $A(n)^{n+}$ and anions $B(8-n)^{n-}$ (Mooser & Pearson, 1956; Birman, 1958). The coexistence of covalent and ionic bonding in sphalerite and wurtzite structure materials has been proven by electron-density determinations (AlN, BeO, ZnO, ZnS) (Jeffrey & Perry, 1955; Jeffrey, Perry & Mozzi, 1956; Jumpertz, 1955) by Reststrahlen absorption (InP, InAs, InSb; GaAs, GaSb; AlSb; ZnS; SiC) (Burstein & Egli, 1955; Picus, Burstein & Henvis, 1956), by the piezo-electric effect (ZnS; CuCl, AgI) (Grimm & Wolff, 1933; Monier & Kern, 1956) and by elastic moduli (Potter, 1957) and cleavage determinations (Wolff, 1954). Interaction between covalent and ionic bonding results in a strengthening of the bond, as compared to 100% covalent or 100% ionic bonding. A high electron mobility follows it (Welker, 1952) and also a relationship between Knoop Hardness H and interatomic distance of the form $H \propto r^{-(m-3)}$. The number m is greatest for the $A(\mathrm{III})B(\mathrm{V})$ and $A(\mathrm{II})B(\mathrm{VI})$ compounds, (Wolff, Toman, Jr., Field & Clark, 1955, 1956). It should not differ much from 1–2 for pure covalent and ionic bonding, where Hxr^{-3} is assumed to be proportional to the lattice energy to a first approximation. These few examples are given to show the co-existence of covalent and ionic bonding in materials of these structures.*

(ii) Ionic and covalent bonding in the surface.

Due to resonance between the possible boundary structures $A^{n+}B^{n-}$ and $A^{(n-4)+}B^{(n-4)-}$ for 100% ionic and 100% covalent bonding, respectively, none of the compounds $A(n)B(8-n)$ could be described by just one of the two boundary formulas given. A seemingly paradoxical situation arises in compound crystals of prevalently covalent character, where the structural elements are not electrically neutral but would appear to be electrically charged or 'pseudo-ionic'. The investigations mentioned in the preceding paragraph will not distinguish between the two possibilities, ionic ($Ga^{3+}P^{3-}$) or 'pseudo-ionic' ($Ga^{-}P^{+}$) which are of opposite sign. They will indicate only the absolute value of q/e but not its electrical sign. Cleavage, in particular, will inform us of the absolute q/e value of the surface atoms, which may well be different from the q/e value of the atoms in the bulk. In the following discussion, these expressions will be given as $(q/e)_{hkl}$ and $(q/e)_{\mathrm{bulk}}$, referring to the plane hkl and the bulk of the crystal, respectively.

If $(q/e)_{hkl}$ is negligible in all planes and in the bulk ('neutral bonding'), (111) cleavage predominates; on the other hand, if $(q/e)_{hkl}$ is appreciably large, (011) cleavage occurs either additionally, or exclusively.

In (111), as well as in (011) cleavage the constituents A and B separate from one of their four original neighbors present in the bulk of the crystal. The atoms retain their effective charge, when the following occur:

1. An 'unshared' or 'ionic' binding electron pair remains with B—or:

2. The two electrons of an originally 'shared' or 'covalent' electron pair separate and stay with A and B.

According to 1 or 2, the condition $(q/e)_{\mathrm{bulk}} = 0$ for 25%, 50% and 75% (or $25(4-n)\%$) ionic bonding character in $A(\mathrm{III})B(\mathrm{V})$, $A(\mathrm{II})B(\mathrm{VI})$ and $A(\mathrm{I})B(\mathrm{VII})$ compounds, respectively, holds true for $(q/e)_{111}$ as well. On the other hand, the effective charge of A and B is changed by $+1$ and -1, respectively, when an originally 'shared' or 'covalent' binding electron pair goes with B. In this case $(q/e)_{\mathrm{bulk}} - 1 = (q/e)_{111} = 0$ when their ionic bonding character is 0%, 25% and 50% (or $25(3-n)\%$), respectively (Fig. 11). In other words the atomic surface charge $(q/e)_{111} = 0$ in GaP, BP etc. when (q/e) bulk $= \pm 1$, i.e. $Ga^{-}P^{+}$, $B^{-}P^{+}$, etc. Therefore, (011) cleavage in $A(n)B(8-n)$ compounds

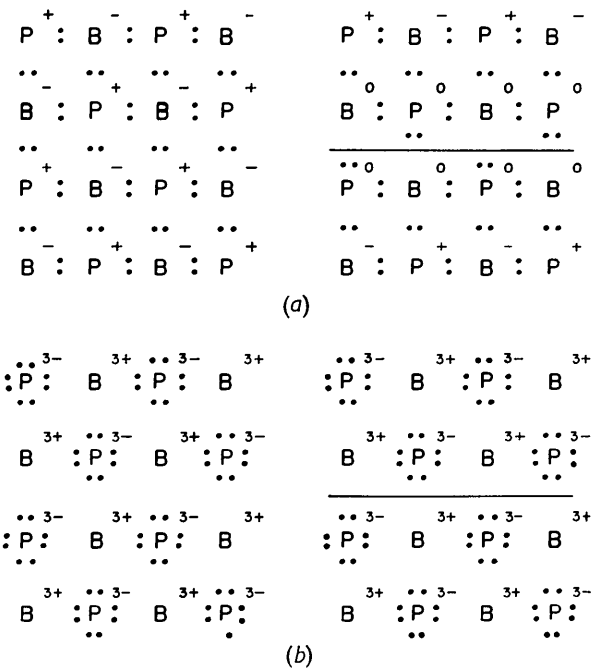

Fig. 11. Schematic figure representing cleavage of BP. Only *one* next nearest neighbor ('bond') of four separates from its partner in hhl ($h \geq l$) for sphalerite structure and in (0001), (10$\bar{1}$0), (11$\bar{2}$0) for wurtzite structure. The cleavage is demonstrated in a schematic drawing for symmetrical electron distribution (100% covalent bonding) and for 100% ionic bonding in Fig. (*a*) and (*b*), respectively. The two phases represent the idealized arrangement of atoms and electrons before and after cleavage. Notice that for 100% covalent bonding in (*a*) the surface atoms acquire 0 electrical charge.

* Faessler & Goehring (1955) find, however, from $K\alpha$ doublet measurements, the ionic character exclusively in the sphalerite.

may be expected when the following relations for the ionic bonding character P, hold: $0 < P < 25(3-n)$ and $100 > P > 25(4-n)$, i.e. when $(q/e)_{hkl} \neq 0$ (P is given in %). Since this cleavage was observed in all investigated $A(n)$ and $B(8-n)$ compounds of sphalerite structure and since a critical study of the magnitude of reported values of $(q/e)_{\text{bulk}}$ and of the results by X-ray Fourier analysis supports the concept of a positive charge for A and a negative charge for B, it can be concluded that the ionic character, P, of the A(III)B(V), A(II)B(VI) and A(I)B(VII) compounds is greater than 25%, 50% and 75%, respectively. Furthermore, since appreciable (111) cleavage was found for InSb, InAs and GaSb, it is concluded that for these compounds P is not very much larger than 29%. This is in fair agreement with Fan's and Burstein's (dynamic) values which indicate 33–34%, 33% and 29% ionic character, respectively, for these compounds.

Accordingly for CdTe, a value near 60% may be concluded from our measurements. The P values for the other compounds are somewhat higher, except for HgSe and HgTe. The presence of (0001) cleavage in SiC, ZnO, ZnS (Birman, 1958), CdS and CdSe forbids assuming too high a q/e value. Rough estimates for CdSe, CdS, ZnS, and ZnO are 60–65%, 65–70%, 67–72% and 75%, respectively.

The results for ZnTe and CdTe seem to indicate that impurities and low resistivity favor (111) cleavage. In this case, electrical charges arising from the two separating (111) cleavage surfaces are neutralized rapidly through contact points which separate last. This is confirmed by photomultiplier investigation of *triboluminescence* of the compounds ZnO, ZnS, ZnSe; CdS, SiC; ZnTe, CdSe, CuI, AgI, GaP, GaAs, GaSb, InP, InAs and InSb. Of this series, only the first five emit light when fractured. This can be explained as follows: when the crystals cleave in (111) and are not conducting, an electrical discharge results between the separating cleavage surfaces (Wolff, 1952). This is expected, since the surface layers of these planes represent A or B layers, respectively (Fig. 12). Opacity of the crystals does not matter, since the discharge can be observed parallel to the cleaving planes.

For $A(n)B(8-n)$ compounds there may be a considerable infrared emission due to electron-hole recombination which cannot be recorded by the photomultiplier. This does not influence the ultraviolet discharge emission. CuI and AgI do not emit light, since these soft materials slip along (111) rather than cleave in this direction. Separation along the major cleavage plane (011) would not be very likely to produce light. The light emission from Si, Ge, GaAs and other crystals during sandblasting (Jenny, 1957) appears to be of a different nature and not triboluminescence as defined in our experiments.

Microcleavage in the planes $(hhl)(h > l)$, *which appears together with the cleavage in* (111) *indicates*

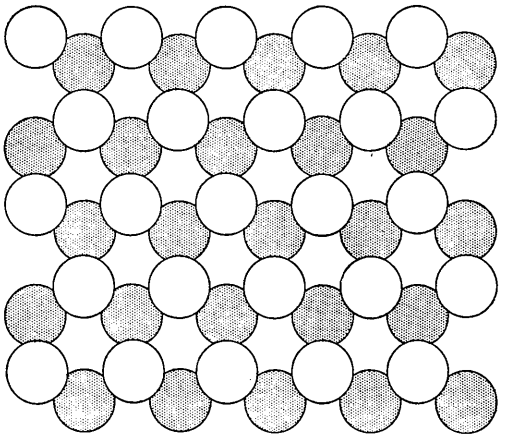

Fig. 12. Top view of a (111) plane of sphalerite or diamond structure crystals or of a (0001) plane of wurtzite structure crystals. The open circles represent the atoms of the upper layer (in compounds of sphalerite structure A atoms with a positive or negative electrical charge) while the shaded circles represent the atoms of the lower layer strongly bonded to the upper layer (in compounds of sphalerite structure B atoms with a charge opposite to the A charge). Both layers represent physically one single and strongly coherent layer.

'neutral' or indirectly covalent bonding. This is apparent, since for this type of bonding, the condition 1, described in Chapter II, holds true that is to say the number of bonds to be separated is at a minimum. For the microcleavage, this means that only the strongly bonded one-dimensional arrays of atoms along the zone (*PBC*-vectors; Hartman & Perdok, 1955) can be separated one from another. The application of condition 2 in Chapter II for *ionic bonding*, namely the presence of an array of atoms with alternate signs of effective charge (q/e), *applies similarly to the microcleavage along the zone* [111] (as the effective direction) *and the plane* (011) (Fig. 13, checkerboard arrangement).

The schematic presentations in Figs. 6 and 7 which indicate increasing (011) cleavage, as compared with microcleavage in (111) and $(hhl)(h \geq l)$, do not seem to conform with electronegativity concepts. According to the electronegativity scale, the group II and III compounds of period 4 (Zn and Ga compounds) possess less ionic bonding character than the corresponding compounds in period 5 (Cd and In compounds) and yet the ratio of (011) to (111) cleavage increases systematically with decreasing period. If this is to be explained on the basis of the validity of the electronegativity scale in these compounds, then it must be assumed that not only the electrical charge of A and B, but also their distance determines the cleavage in (011). When the interatomic distance is small enough to cause the electrostatic repulsion to be appreciable, this would overcompensate the decrease of ionic character and (q/e) of the Zn and Ga compounds as compared to the Cd and In compounds.

There is no difference in cleavage to be found in wurtzite structure materials, with respect to difference due to ionic and 'neutral' (or indirectly covalent) bonding. This result is supported by the cleavage found in hexagonal ice, the structure of which is the prototype for a wurtzite structure crystal with (nearly) 'neutral' bonding.

(iii). Surface deformation.

The third type of cleavage, found in HgTe, HgSe and CdTe, suggests that the surface of crystals having this type of cleavage is deformed so that the atoms of the first, and possibly to a minor extent the second surface layer, shift to new equilibrium positions; this would be especially true for the (001) plane. The atoms in the upper (001) surface layer shift from the normal tetrahedral positions in the diagonal direction by one-fourth of the lattice diagonal. They are each placed between four of the atoms of the second surface layer. Thus, the arrangement of the atoms in the (001) surface approaches the NaCl arrangement. Only this arrangement would result in a microcleavage in (001) and parallel to [100] if the atoms carry electrical (ionic or 'pseudo-ionic') charges. The strong bonding within the arrays of atoms parallel to $[1\bar{1}0]$ in this case is missing. The fourfold tetrahedral arrangement changes to a more rectangular and octahedral NaCl(PbS) arrangement with sixfold coordination, which likely corresponds to a partial change from sp^3 hybrid bonding to p bonding. This hypothesis is supported by the fact that such behavior is observed solely in crystals which have 'cations' of low polarization and high polarizability (Cd and Hg) that are able to form compounds of NaCl or NaCl-like structure with partial p-bonding or related bonding (CdO and HgS (cinnabar)). In view of this, it is interesting to note that there is $(11\bar{2}0)$ microcleavage in both hexagonal CdS and CdSe, in addition to (0001) and $(10\bar{1}0)$ cleavage, but no $(11\bar{2}0)$ cleavage in hexagonal ZnO and ZnS. This can be interpreted as due to surface deformation as in the case of the sphalerite structure. $(11\bar{2}0)$ can be distorted sufficiently for it to appear as a distinct cleavage.

The (001) surface structure as found in HgTe, HgSe and CdTe is likewise related to the $B-10$ (PbO) structure present in InBi. In these structures, only half of the atoms (Hg and Bi) as compared to the (001) layer in sphalerite or NaCl, occupy the positions in a layer. It is expected that a surface structure intermediate between the NaCl and PbO layer structures results, in such a way that half of the surface atoms occupy positions on a normal, centered between four neighboring atoms of the second layer, and at a short distance from the second layer.

(iv) Bonding in chalcopyrite.

Another type of cleavage is found in chalcopyrite, $CuFeS_2$, which is structurally related to sphalerite. The microcleavage parallel to [111] ([112] in cubic notation) corresponds to the strongly bonded atomic array FeSFeS. This is illustrated by cleavage at the intersection of two such zones in (011) (cubic notation (021)), where for four bonds to be separated, three weak CuS bonds and only one strong FeS bond are involved. In general, the ratio of CuS/FeS bonds is less than three but greater than one for planes in the zone [111]. Thus, this type of cleavage and microcleavage indicates the weakness of one bond, (probably CuS), with respect to the other (FeS).

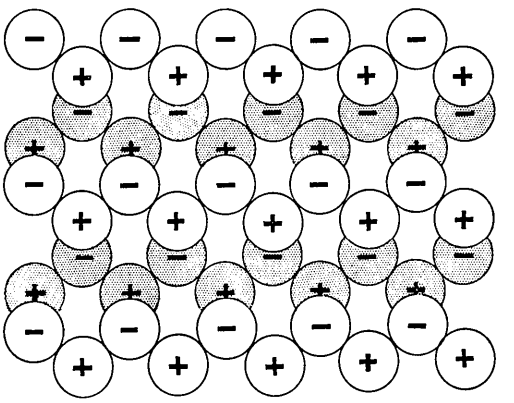

Fig. 13. Top view of an (011) plane of the sphalerite structure. The open circles represent the upper atomic layer and the shaded circles represent the next lower layer. Electrical charges may also be present in diamond structure materials; the charges are effectively limited to the upper layer and are not fixed in corresponding atoms but form a resonating system. Thus, this would tend to stabilize the (011) plane in diamond structure crystals.

Fig. 13 is used to explain why chalcopyrite shows cleavage in (110) but not in (012) (cubic notation: (011)). The open circles represent arrays of atoms as part of a crystal above the figure. This crystal is to be separated within the (110) plane from the underlying part of the crystal with the shaded circles as the upper layer. The shaded circles also represent arrays of atoms of alternate electrical sign. In order to have appreciable cleavage that is due to ionic character, the open circle arrays have to be moved with respect to the shaded circle arrays in the $[\bar{1}11]$ and $[1\bar{1}1]$ directions (cubic notations). If the coherence of the atomic arrays is strong, the cleavage will be distinct and perfect. In sphalerite, for example, the atomic arrays will be arrays of Zn–S–Zn atoms. In chalcopyrite, the arrays will be given either by a S–Cu–S–Fe–S–Cu–S–Fe sequence or by a sequence S–Cu–S–Cu–S–Fe–S–Fe–S–Cu–S–Cu etc. depending upon whether the plane is (110) or (012) (cubic notation: (011)). It appears plausible that the first sequence is much stronger in bonding than the second, since in the first case the sulphur atom balances the binding electron distribution between the atoms better than it does in the second sequence.

(*b*) *Fluorite-structure materials*

A difference in surface structure, similar to that exhibited by the cleavage in sphalerite-structure materials, is found in crystals of the fluorite structure, CaF_2 and Mg_2Sn. Both display the type 2 microcleavage pattern which is also to be found in sphalerite-structure crystals. $AuGa_2$ and $AuIn_2$ display Type 2, together with Type 3, however, as does CdTe. A similar effect is expected in Mg_2Pb.

No difference is found in cleavage with respect to ionic and 'neutral' (or indirectly covalent) bonding. There is insufficient repelling action between electrically charged atoms of opposite sign for the shift in the $[11\bar{1}]$ direction to occur. A shift of the atomic arrays in the [011] direction is, therefore, the only cause of cleavage in (011); the cleavage in (011) is not distinct as it is in InSb (Figs. 4 and 6), but rather indistinct as it is in diamond (Figs. 6(*a*), 11).

(*c*) *Diamond-structure materials*

(i) Cleavage and surface structure.

The cleavage in diamond (Fig. 6(*a*)) corresponds to ideal covalent bonding and to a non-deformed surface such as is present in the molecular diamond-structures of arsenolite and senarmontite. These substances are built up of rigid molecules As_4O_6 and Sb_4O_6 and show the same cleavage pattern as diamond (Figs. 5(*b*), versus 5(*a*)). Ionic bonding between the molecules of these compounds have a negligible effect on cleavage.

Si and Ge each display a different cleavage, however. An examination of the circumstances leads to the following explanation of what causes this difference: in the $[1\bar{1}0]$ zone in Si and Ge of diamond structure, the surface layer of the planes between (111) and (001) is deformable appreciably. Therefore, the specific surface energy of these planes can be lowered sensibly as compared to a possible small change of the surface energy of the planes between (111) and (110). In the unchanged, ideal diamond structure surface, there are two maxima of the specific surface energy in (001) and (110) in the $[1\bar{1}0]$ zone; the higher being in (001). The reverse is probably true in Si and Ge, due to the change in surface structure which results in the (001) maximum value being lower than the (110) value. As a first approximation for an unchanged surface structure the specific surface energy σ_{hkl} at 0 °K. is proportional to the number N_{hkl} of 'free' bonds between first nearest neighbors per unit area a_0^2. The symbol a_0 represents the lattice constant. For $0 \leq h \leq l$ and $0 \leq k \leq l$ this number is given by

$$N_{hkl} = N_{001} \times l/(h^2+k^2+l^2)^{\frac{1}{2}}$$

hkl	(001)	(113)	(112)	(111)	(122)	(011)
N_{hkl}	4·00	3·62	3·26	2·31	2·67	2·82

For ideal diamond structure crystals, N_{hkl} values for the planes hkl in the region between (111) and (110) on the $[1\bar{1}0]$ zone are smaller than the values of the planes between (111) and (001). In a crystal of diamond structure with ideal covalent bonding and an undistorted surface structure, little cleavage in the latter region would be expected. This can be explained, in simple terms, as follows: any cleavage and microcleavage in (*hkl*) produces terraced (111) planes of molecular dimension. The step boundaries of unit height, $a_0/\sqrt{3}$ are of two types: (*a*) steps appearing in (*hhl*) planes with $h > l$; the atoms along the surface of the '*a*-steps' have been separated from only one neighboring atom of the original four neighboring atoms in the bulk crystal; (*b*) steps appearing in (*hhl*) planes with $h < l$; the atoms along the surface of the '*b*-steps' have two neighboring atoms missing. It is therefore, more difficult to produce (*hhl*) planes with '*b*-steps' than with '*a*-steps' in a diamond-structure material with an ideal undistorted surface structure; *unless* during the cleavage process the energy necessary to produce an undistorted surface is lowered by a simultaneous atomic rearrangement or by a collapse of the surface structure. The described *a*-cleavage and *a*-steps occur in diamond, As_4O_6 and Sb_4O_6; therefore, each may have a nearly ideal surface, while Si and Ge show *b*-cleavage and *b*-steps indicating a collapse and deformation of the surface structure.

Outside the $[1\bar{1}0]$ zone, very little cleavage is to be expected, since an exponential relationship of exposed surface area and specific surface energy for the different (*hkl*) planes is indicated. The surface energy for (013) for instance, would be 3·73 which is high when compared with the values previously mentioned.

Polarization causes a change in the surface structure from the ideal structure. This change corresponds to the change from tetrahedral, or directional bonding to spherical, or undirected bonding. A simple calculation will show, then, that the surface energy is lowered. This will be done in two ways: (1) the interaction of the atoms is proportional to r^{-6}. σ_{001} is lowered by a factor of approximately 0·6 when interactions up to the second or third nearest neighbors are taken into account; (2) a more reasonable assumption for diamond (for strictly directional bonding) is to neglect all but the first nearest neighbor interaction and take into account the energy of deformation of the bond angle from the tetrahedral arrangement. This can be estimated by interpolation of the bond angle deformation energy of cycloalkanes. Thus, a surface energy reduction factor of about 0·85 results. Here the surface structure of (001), as shown in Fig. 14, changes to the arrangement given in Fig. 15. This structure has also been proposed by Schlier & Farnsworth (1956; Farnsworth & Schlier, 1958) for Si and Ge in the interpretation of their results on low-energy diffraction from Si and Ge surfaces.

The factor 0·85 would not reduce σ_{001} below the ideal (011) value to cause appreciable (001) cleavage. Any additional interaction and rearrangement of the surface atoms of the upper layers would, however, result in such an effect. This seems to be true, since

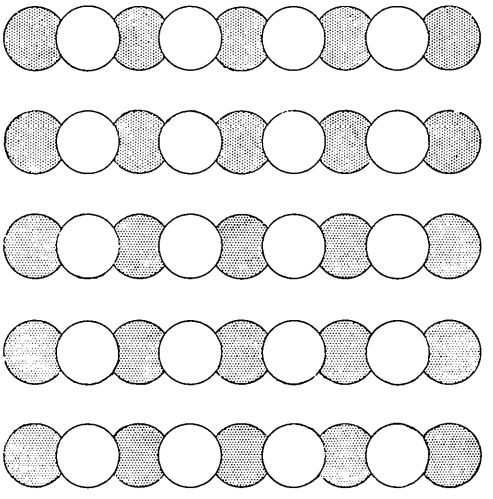

Fig. 14. Ideal arrangements of atoms in (001). The open and shaded circles represent the atoms of the upper and lower layers, respectively; in sphalerite structure materials they are of opposite charges as indicated (top view).

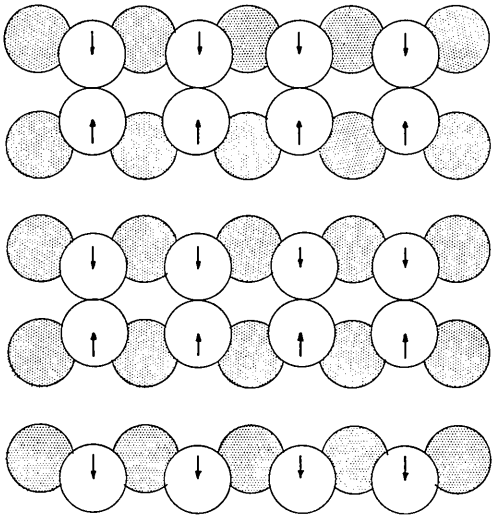

Fig. 15. The arrangement of the atoms in (001) after the structure change when the atoms of the upper layer approach each other (see arrows) and thus partially saturate 'free bondings' (top view).

the cleavage patterns of Si and Ge on the one hand, and of diamond on the other, differ so much. The probable structure is suggested by the cleavage pattern as observed for HgSe and HgTe which for Si and Ge would mean a surface layer of nearly simple cubic structure (lattice constant $a_0/\sqrt{2}$; Fig. 16) as approached in β-Sn. A similar indication of a tendency toward the formation of octahedral coordination, and likely p-bonding, is found in the sequence of the group Vb elements, As, Sb, Bi.

The doubling of the diagonal lattice spacings in the [110] direction found by low-energy electron diffraction (Schlier & Farnsworth, 1956; Farnsworth & Schlier, 1958) indicates a surface deformation on (001) and accounts, by the concept of half a monolayer, for the number of binding electrons available from the atoms in the second layer. It also explains the appearance of the (001), (113) and (013) planes in the equilibrium forms of Si and Ge and, in particular, the predominance of the (113) plane with respect to the other planes mentioned.

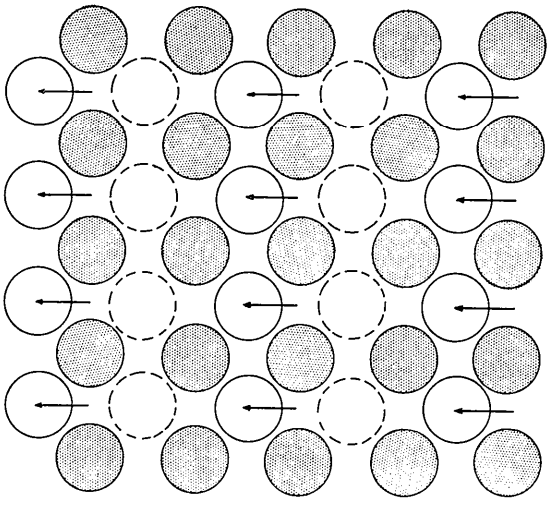

Fig. 16. The arrangement of atoms in (001) after the structure change when the atoms move into positions between or slightly above the centers of the underlying shaded atoms (see arrows). The atoms as shown by the dotted circles are very probably missing as low-energy electron diffraction data indicate (double spacing in [110]) (Schlier & Farnsworth, 1956; Farnsworth & Schlier, 1958) (top view).

(ii) Equilibrium form and surface structure.

In the equilibrium forms of Si and Ge, (Wolff, 1956) namely, (111), (001), (113), (011), (013),* a preference for (113) exists. On the other hand, in the equilibrium form of diamond ((111), (001), (011)), the (113) plane appears very rarely. The (*hhl*) plane ($h < l$) is composed of deformed (001)–(111) steps of molecular dimensions ('*b*-steps') and these are oriented arrays of sites of Si or Ge atoms which are alternately occupied and empty. (113) has the highest concentration of deformed steps and occupied sites. Therefore, in addition to (111), the (113) plane corresponds to a cusp in the spherical plot of the surface energy diagram and consequently it appears in the equilibrium form. The sequence of the equilibrium planes in diamond structure crystals (Stranski, 1949) as implied by first—(111); second—(001); third—(011), (113); and fourth—(013) nearest neighbor interaction, respectively, would indicate fairly good agreement with the sequence as obtained in Si and Ge. On the other hand, the concept of the distant neighbor interaction

* The same planes, in addition to (112) are observed in the field emission from Si single crystals (D'Asaro, 1958).

does not explain the reversal, (113), (011), of the planes from the expected sequence in Si and Ge and the rare appearance of (113) in diamond.

The presence of (001) in diamond can be explained easily by the deformation in this plane as suggested by Farnsworth *et al.* (1958) and the authors. The presence of (011) in the equilibrium forms of Si, Ge, diamond, As_4O_6, Sb_4O_6 is the result of a change in surface energy caused by surface deformation or adsorption. Low energy electron diffraction data point to deformation.

6. Materials

Single crystals or oligocrystals of the different materials were obtained from various sources or prepared as indicated. Grown from melt: GaAs, GaSb, InAs, InSb, InBi, ZnTe, CdTe, CuI, Ga_2Te_3, In_2Te_3, $HgIn_2Te_4$, PbS, PbSe, PbTe, SnSe, ice. Crystallized from metallic solution: AlP, AlAs, GaP, $AuGa_2$, $AuIn_2$, $NiIn_2$. Grown from vapor phase: As_4O_6 (200 °C.), Sb_4O_6 (560 °C.), HgSe (500 °C.). Hexagonal AgI crystals grown by diffusional crystallization at the interface of a concentrated KI–AgI solution and water over a period of a month.

Ice crystals grown from the vapor phase were found in a shed in Greenland. They were large plates (5 cm. diameter, displaying growth spirals) and long columns (10 cm.), grown apparently, through the habit modifying effect of fuel vapors. Crystals sponsored: ZnSe, ZnTe, HgS(Cd); InP (R. H. Bube, E. L. Lind; D. A. Jenny, RCA, Princeton, N. J.). ZnS (hex.); CdSe; HgTe (A. Kremheller; O. A. Weinreich; A. R. Liboff, Sylvania Electric Products, Inc., Flushing, Bayside, N. Y.). AlSb, InAs, Ga_2Te_3 (A. C. Beer, E. Paskell, Batelle Memorial Institute, Columbus, Ohio); HgS (metacinnabarite; C. Frondel, 12 Geology Museum, Cambridge, Mass.; P. M. Bethke, Missouri School of Mines, Rolla, Mo.); Cu_3SbS_3, Cu_3AsS_3 (tetrahedrite, Smithsonian Institute, Washington, D. C.; H. O'Daniel, Fischer, Mineral. Institute, Frankfurt, M.); InP (H. Welker, Forschungs-Laboratorium, Siemens-Schuckertwerke, Erlangen); ZnO (zincite; S. S. Goldich, Univ. of Minnesota, Minneapolis) $CuFeS_2$ (chalcopyrite; Museum of Natural History, N.Y.C.); diamond (George Kaplan, Leo Kaplan, Lazare Kaplan, Inc., N.Y.C.), Mg_2Sn (H. P. R. Frederikse, National Bureau of Standards, Washington, D.C.); CdS (W. E. Medcalf, R. H. Fahrig, Eagle-Picher Research Laboratories, Miami, Oklahoma); ZnS (hex.; L. C. Greene, Wright-Patterson AFB, Ohio); Si, Ge; ZnS (cubic); CdS (hex.); LiF, NaCl, KBr, CaF_2 (fluorite); (W. B. Pharo, W. R. Cherry; L. Toman, Jr., J. M. Stanley, P. J. Bramhall; W. W. Malinofsky, U. S. Army Signal Research and Development Laboratory, Fort Monmouth, N. J.).

The authors wish to express their appreciation to those who furnished crystals for this study and are especially grateful to Dr J. A. Kohn, for performing indispensable X-ray (Laue) tests of cleavage planes, to Dr F. W. Leonhard and F. R. Anderson, for the electron micrographs. Drs J. A. Kohn, H. H. Kedesdy and A. A. Giardini were particularly helpful in giving constructive criticism of the manuscript. Thanks are also due to Drs W. B. Pearson, E. Mooser, National Research Council, Ottawa, J. W. Davisson, Naval Res. Lac., Wash., D.C., and J. L. Birman, Sylvania Electric Products, Inc., Bayside, N.Y., for their stimulating discussions.

Note added in proof: Recently, macroscopic single crystals of grey tin have been grown (Ewald & Tufte, 1958). These crystals show distinct (111) cleavage, and distinct microcleavage between (111) and (001) when cleaved at liquid nitrogen temperature (their habit: (111), (001), (113), (137)). The conclusion arrived at for Si and Ge, therefore, also applies to α-Sn (Crystals through the courtesy of Dr A. W. Ewald).

References

Birman, J. L. (1958). *Phys. Rev.* **109**, 810.
Bond, W. L. (1951). *Rev. Sci. Instrum.* **22**, 344.
Burstein, E. & Egli, P. H. (1955). *Advances in Electronics*, **7**, 24.
D'Asaro, L. A. (1958). *J. Appl. Phys.* **29**, 33.
Dewald, J. F. (1955). Electrochem. Soc. Meeting, Enlarged Abstracts, Electronics Div., p. 210.
Dewald, J. F. (1957). *J. Electrochem. Soc.* **104**, 244.
Ewald, A. W. & Tufte, O. N. (1958). *J. Appl. Phys.* **29**, 1007,
Faessler, A. & Goehring, M. (1955). *Z. Phys.* **142**, 558.
Farnsworth, H. E. & Schlier, R. E. (1958). *Bulletin Amer. Phys. Soc.* Ser. II, **3**, 30.
Goodman, C. H. L. (1954). *Proc. Phys. Soc.* B, **67**, 258.
Goodman, C. H. L. (1955). *J. Electronics*, **1**, 115.
Grimm, H. G. & Wolff, H. (1933). *Handbuch d. Phys.* **24**, II, 997.
Hartman, P. & Perdok, W. G. (1955). *Acta Cryst.* **8**, 49, 529.
Jeffrey, G. A. & Perry, G. S. (1955). *J. Chem. Phys.* **23**, 406.
Jeffrey, G. A., Perry, G. S. & Mozzi, R. L. (1956). *J. Chem. Phys.* **25**, 1024.
Jenny, D. A. (1957). *J. Appl. Phys.* **28**, 1515.
Jumpertz, E. A. (1955). *Z. Elektrochem.* **59**, 419.
Mitrenin, V. P. & Alexandria, B. V. (1957). *Growth of Crystals, Academy of Science USSR*, p. 170. (English translation by Consultants Bureau, Inc., 1958, p. 135).
Monier, J. C. & Kern, R. (1956). *Bull. Soc. Franç. Minér. Crist.* **79**, 495.
Mooser, E. & Pearson, W. B. (1956). *J. Electronics*, **1**, 629.
Pfister, H. (1955). *Z. Naturforsch.* **10** a, 79.
Picus, G. S., Burstein, E. & Henvis, B. W. (1956). Second Symp. on Phys. of Semiconductors, Wash., D.C.
Potter, R. F. (1957). *J. Phys. Chem. Solids*, **3**, 223.
Ramaseshan, S. (1946). *Proc. Indian Acad. Sci.* p, 114.
Schlier, R. E. & Farnsworth, H. E. (1956). *Semiconductor Surface Physics*, p. 3. Univ. of Penna. Press.

SPITZER, W. G. & FAN, H. Y. (1955). *Phys. Rev.* **99**, 1892.
STRANSKI, I. N. (1949). *Disc. Faraday Soc.* **5**, 13.
SZIGETI, B. (1949). *Trans. Faraday Soc.* **45**, 155.
VAN WIERINGEN, J. S. (1955). *Disc. Faraday Soc.* **19**, 118.
WELKER, H. (1952). *Z. Naturforsch.* **7** a, 744.
WINKLER, H. G. F. (1950). *Structure and Properties of Crystals*, p. 219. Berlin: Springer.
WOLFF, G. A. (1952). *Proc. Internat. Symposium on Reactivity of Solids*, p. 253. Gothenburg.
WOLFF, G. A. (1954). Electrochem Soc. Meeting, Electronics Div., Enlarged Abstracts, p. 101.
WOLFF, G. A., TOMAN, L., JR. & CLARK, J. C. (1955). *Phys. Rev.* **98**, 1179.
WOLFF, G. A. (1956). *Amer. Min.* **41**, 60.
WOLFF, G. A., TOMAN, L., JR., FIELD, N. J. & CLARK, J. C. (1956). *Proc. Internat. Colloquium on Semiconductors and Phosphors Garmisch*, p. 463.
WOLFF, G. A., WILBUR, J. M., JR. & CLARK, J. C. (1957). *Z. Elektrochem.* **61**, 101.
ZAPFFE, C. A. & WORDEN, C. O. (1949). *Acta Cryst.* **2**, 377.

Acta Cryst. (1959). **12**, 323

The Crystal Structure of P_4Se_3

BY E. KEULEN AND AAFJE VOS

Laboratorium voor Anorganische en Fysische Chemie der Rijksuniversiteit Groningen, The Netherlands

(*Received* 28 *June* 1958 *and in revised form* 29 *September* 1958)

P_4Se_3 belongs to the same space group as the low-temperature modification of P_4S_3. Its crystal structure, by analogy to that of the latter compound, consists of molecules P_4Se_3. In both compounds the molecules are located on the planes of symmetry, but their arrangement in these planes is different. The unit cell of P_4Se_3 is twice as large as that of P_4S_3. The orientation and the position of the molecules was found by interpretation of the [100] and [010] Patterson synthesis combined with trial and error. The co-ordinates were refined by computing Fourier syntheses of the [100] and [010] projection. The average P–P and P–Se bond lengths are 2·25 and 2·24 Å with an e.s.d. of 0·03 and 0·01 Å respectively. The average values of the valence angles Se–P–Se, P–Se–P, Se–P–P and P–P–P are 99·9°, 100·1°, 105·3° and 60·1° respectively. The standard deviation in the individual valence angles is about 1°. Shortest intermolecular distances—about 3·6 Å—are observed between phosphorus atoms.

Introduction

Two phosphorus–selenium compounds, P_4Se_3 and P_2Se_5, have been reported in the literature (Mai, 1928; Robinson & Scott, 1933; Haq & Samuel, 1937; further references are given in these papers). According to Mai (1926) P_4Se_3 possibly exists in two modifications.

An X-ray investigation of the crystal structures of the phosphorus selenides was undertaken with the object of comparing the structures of these compounds with the recently determined structures of the corresponding sulfides (Vos & Wiebenga, 1955; Leung *et al.*, 1957); P_4Se_3 was investigated first.

Experimental

Materials

P_4Se_3 was prepared by heating white phosphorus and selenium in tetralin (Mai, 1928). The solid reaction product was extracted with tetralin and from the solution thus obtained P_4Se_3 was precipitated by cooling or by addition of ether. After purification by crystallization from benzene, the melting point agreed with the value reported by Mai (242 °C.). Crystals were grown by slowly cooling the solution in benzene. As the crystals are not stable in moist air, they were transferred into a borosilicate glass capillary in which they could be kept for a long time. Perpendicular to the crystal axis about which the photographs were made, their diameter was approximately 0·1 mm.

Unit cell and space group

Oscillation and Weissenberg photographs, which were made of a number of layer lines about the *b*-axis, indicated an orthorhombic symmetry for the P_4Se_3 crystals. The systematic absences observed were $h0l$ with $h+l$ odd and $hk0$ with k odd, which indicated as probable space group either $Pmnb$ or $P2_1nb$. Because of the absence of piezoelectricity, the crystals were assumed to belong to the centrosymmetric space group $Pmnb$, which was confirmed during the structure analysis. The lattice constants were determined accurately from back reflexion photographs. In Table 1 the lattice constants of P_4Se_3 are compared with those of P_4S_3 (Leung *et al.*, 1957). With 16 units of P_4Se_3 per unit cell the calculated density, 3·17 g.cm.$^{-3}$, was